Continuous Single-Phase Synthesis of [$Au_{25}(Cys)_{18}$] Nanoclusters and their Photobactericidal Enhancement

Gi Byoung Hwang[at], Gaowei Wu[bt], Juhun Shin[a], Luca Panariello[b], Victor Sebastian[c]

Kersti Karu[a], Elaine Allan[d], Asterios Gavriilidis[b]*, and Ivan P. Parkin[a]*

[a] *Materials Chemistry Research Centre, Department of Chemistry, University College London, 20 Gordon Street, London, WC1H 0AJ, United Kingdom*

[b] *Department of Chemical Engineering, University College London, Torrington Place, London, WC1E 7JE, United Kingdom*

[c] *Nanoscience Institute of Aragon, Aragón Materials Science Institute, ICMA, CSIC and Chemical and Environmental Engineering Department, University of Zaragoza, 50018 Zaragoza, Spain*

[d] *Department of Microbial Diseases, UCL Eastman Dental Institute, Royal Free Campus, University College London, Rowland Hill Street, London, NW3 2PF, United Kingdom*

[t] These authors contributed equally
[*] corresponding author
Asterios Gavriilidis, E-mail: a.gavriilidis@ucl.ac.uk

Ivan P. Parkin, E-mail: i.p.parkin@ucl.ac.uk

ABSTRACT

Thiolate-gold nanoclusters have various applications. However, most of the synthesis methods require prolonged synthesis times from several hours to days. In the present study, we report a rapid synthesis method for $[Au_{25}(Cys)_{18}]$ nanoclusters and their application for photobactericidal enhancement. For $[Au_{25}(Cys)_{18}]$ synthesis, we employed a tube-in-tube membrane reactor using CO as a reducing agent at elevated temperatures. This approach allows continuous generation of high quality $[Au_{25}(Cys)_{18}]$ within 3 min. Photobactericidal tests against *Staphylococcus aureus* showed that crystal violet treated polymer did not have photobactericidal activity, but addition of $[Au_{25}(Cys)_{18}]$ in the treated polymer demonstrated a potent photobactericidal activity at a low white light flux, resulting in > 4.29 log reduction in viable bacteria number. Steady state and time-resolved photoluminescence spectroscopies demonstrated that after light irradiation, photoexcited electrons in crystal violet flowed to $[Au_{25}(Cys)_{18}]$ in the silicone, suggesting that redox reaction from $[Au_{25}(Cys)_{18}]$ enhanced the photobactericidal activity. Stability tests revealed that leaching of crystal violet and $[Au_{25}(Cys)_{18}]$ from the treated silicone was negligible and cyclic testing showed the silicone maintained a strong photobactericidal activity after repeated use.

KEYWORDS: $[Au_{25}(Cys)_{18}]$, gold nanocluster, *Staphylococcus aureus*, bactericidal activity, crystal violet, photocatalyst, continuous flow, membrane reactor

1. INTRODUCTION

In recent years, metal nanoclusters have attracted attention in nanoscience due to their unique physico-chemical properties [1-2]. The nanoclusters typically consist of ten to several hundred atoms and their size is often <2 nm [1-2]. Metal nanoclusters are synthesized with consideration of the delicate balance between cluster growth and etching and they are essentially organic/inorganic hybrid nanomaterials [1-3]. Because of their ultra-small size, the nanoclusters are a bridge between small molecules and plasmonic metal nanoparticles and they exhibit a strong quantum size effect, for example distinct energy levels of electrons, extraordinary nonlinear optical properties and catalytic chemical reactivity [4]. Thus, metal nanoclusters have a great potential for application in catalysis, biomedicine and energy conversion [1-2, 4]. In the last decade, size control of gold nanoclusters was studied and various monodisperse gold nanoclusters were reported [1-2, 4]. Among them, Au_{25} nanoclusters with Au_{13} core and exterior part consisting of twelve Au atoms and eighteen ligands (Figure S1) have been extensively studied due to facile synthesis, high stability, and ease of functionalization[1].

A sodium borohydride ($NaBH_4$) reduction method has been commonly utilized for synthesis of thiolate Au_{25} nanoclusters [5-7]. In this method, $NaBH_4$ reduction on Au (I) complexes produces polydisperse Au nanoclusters and slow etching of the nanoclusters by excess thiolate ligand causes the transformation of the multi-sized nanoclusters into mono-sized ones (size focusing) [3, 7-10]. The synthesis time for formation of Au_{25} nanoclusters has ranged from few hours to days for size evolution and focusing [11-12]. Recently, it was shown that during size focusing of Au_{25} nanoclusters, heat treatment is the most efficient way to speed up the reaction process and it can facilitate the transformation of multi-sized nanoclusters into the more thermodynamically stable Au_{25} nanoclusters [6]. Katla et al. reported a single step $[Au_{25}(GSH)_{18}]$ (GSH = L-glutathione) synthesis at 60 ^oC to accelerate the reaction process, resulting in a reduction of reaction time to 2 h [7]. In $[Au_{25}(MHA)_{18}]$ (MHA = 6-mercaptohexanoic acid)

synthesis, the Xie group used sodium hydroxide (NaOH) to decrease the reduction ability of $NaBH_4$ and enhance the etching ability of the free thiolate ligands resulting in rapid formation of the nanoclusters [3]. Further study showed that a mild heat treatment of the reaction solution accelerated the thermodynamically stable $[Au_{25}(MHA)_{18}]$ formation, resulting in high yield (>95%) of the nanocluster [3, 6].

With the continuing emergence of antibiotic resistant bacteria, use of photobactericidal materials is considered a promising alternative to kill bacteria because the bactericidal mechanism of the photocatalysts is different from that of antibiotics [13]. Photocatalysts containing titanium dioxide (TiO_2), zinc oxide (ZnO) and photosensitizers containing toluidine blue O (TBO), methylene blue (MB) and crystal violet (CV) were extensively studied and they showed broad bactericidal activity on light irradiation [14-19]. However, they require UV-activation or use of a laser with wavelength between 400-800 nm in order to show photobactericidal activity [14-19]. In order to enhance the photocatalytic reaction, photocatalytic nanocomposites using carbon nanotubes (CNT), silver (Ag) and gold (Au) nanoparticles (NPs) were studied [20-24]. It was shown that CNT or Ag NPs doped on UV-active photocatalysts produced photobactericidal activity upon irradiation of visible light with intensity of >0.2 mW/cm^2 and that Au or Ag NPs addition to the photosensitizers produced a potent photobactericidal activity after exposure to white light with >0.15 mW/cm^2 (>1000 lux) [20-25].

Although many techniques of photobactericidal enhancement by metal nanoparticles were suggested, most of them require an intense light (>1000 lux) or a laser source to obtain a satisfactory bacteria kill, indicating that the techniques can only be effective in facilities with extremely bright light sources such as surgical site and emergency room[20-25]. In this study, a tube-in-tube membrane reactor was employed where carbon monoxide (CO) as a gaseous reducing agent and heat treatment were used to accelerate the synthesis of thermodynamically

stable [$Au_{25}(Cys)_{18}$] (Scheme 1). Our method showed that [$Au_{25}(Cys)_{18}$] with high purity can be synthesized within 3 min residence time under heat treatment and continuous synthesis for 8 h, indicating that it is capable of large-scale production of [$Au_{25}(Cys)_{18}$]. [$Au_{25}(Cys)_{18}$] was utilized to enhance photobactericidal activity of a crystal violet sensitizer, when both were incorporated into a polymer surface. Bactericidal tests against *Staphylococcus aureus* showed that [$Au_{25}(Cys)_{18}$] significantly increased the photobactericidal activity of the polymer at very low flux of white light (312 lux average).

2. EXPERIMENTAL SECTION

2.1. [$Au_{25}(Cys)_{18}$] Synthesis and Characterization. 45.5 mg (0.38 mmol) of L-cysteine was added in 5 mL of DI water, 9.9 mL of chloroauric acid solution ($HAuCl_4$, 25.2 mM) and 0.833 mL of sodium hydroxide solution (NaOH, 2 M) were added to the cysteine solution. After that, 9.267 mL of DI water was added into the mixture. The final concentrations of the various reactants in the Au precursor solution were: [$HAuCl_4$] = 10 mM, [L-cysteine] = 15 mM, [NaOH] = 66.64 mM. The schematic of the tube-in-tube membrane reactor utilized in this work is shown in Figure 1. The membrane reactor consisted of an inner Teflon AF-2400 tube acting as membrane (outer diameter (OD): 1.0 mm, inner diameter (ID): 0.8 mm, Biogeneral) and an outer PTFE tube (OD: 3.2 mm, ID: 2.4 mm, VICI Jour). The length of the membrane reactor was 2 m, and the volume of the Teflon AF-2400 tube in the reactor was 1 mL. The Au precursor solution was delivered at 0.33 mL/min to the Teflon AF-2400 tube with a milliGAT LF pump (VICI Valco), and a back pressure regulator (BPR, Zaiput) was connected to the outlet of the reactor. The solution was collected at the outlet of the BPR. The liquid pressure in the inner tube was maintained by the BPR and measured with a pressure sensor (LTF) placed at the inlet of the inner tube. A gaseous CO supply was connected to the inlet of the annulus between the inner and outer tubes by a T-junction (IDEX), and another T-junction was used at the outlet of the annulus to enable the release of the pressurized CO after the experiment. The pressure of

the CO was controlled by a gas pressure regulator (Swagelok, K series) and monitored with a pressure sensor (40PC150G, Honeywell). During the experiment, the gas and liquid pressures were maintained at 4 barg and 5 barg, respectively. The reactor was heated with an oil bath, and the temperature of the oil bath was measured and controlled by a hotplate (IKA, RCT basic).

UV-Vis absorbance spectrum of the collected [$Au_{25}(Cys)_{18}$] solution was determined by an Ocean Optics UV-Vis-ES spectrometer (USB 2000+ Spectrometer and DT-Mini-2-GS light source) after diluting the collected solution with H_2O by a factor of 10. Electrospray ionization mass spectrometry (ESI-MS, Agilent 6510 Q-TOF MS) was utilized to identify the molecular mass of the Au clusters. Dried [$Au_{25}(Cys)_{18}$] nanoclusters were mixed with DI water including 0.01 µM cesium acetate, and then the mixture was injected into the ESI-MS at 20 µL/min. The ESI was performed at negative mode. Heated nitrogen gas was supplied to the mass spectrometer at 5 L/min. The negatively charged ions were analyzed by the spectrometer.

2.2. Production of Photobactericidal Silicone through a Swell-Encapsulation-Shrink Process. Photobactericidal silicone was produced by a swell-encapsulation-shrink process as depicted in Scheme 2. Prior to the production of the photobactericidal polymer, [$Au_{25}(Cys)_{18}$] solution was 3-fold diluted.

2.2.1. Control: A silicone coupon (4.5 cm × 7.0 cm × 0.04 cm, cut from a universal desktop keyboard skin protector cover, Universal, China) was immersed in a mixture of acetone (140 mL) and DI water (140 mL) for 24 h. The silicone was washed by DI water twice and after that, it was stored in dark room for 24 h.

2.2.2. Silicone Containing [$Au_{25}(Cys)_{18}$]: A silicone coupon was immersed in a mixture of [$Au_{25}(Cys)_{18}$] solution (28 mL), DI water (112 mL) and acetone (140 mL) for 24 h and then it was washed by DI water twice. After that, the silicone was stored in dark room for 24 h.

2.2.3. Silicone Containing Crystal Violet: 224 mg of crystal violet was dissolved in a mixture of DI water (140 mL) and acetone (140 mL) and it was sonicated for 3 min. After that, the silicone coupon was immersed in the mixture for 24 h. Subsequently, the silicone was washed using DI water twice and it was stored in dark room for 24 h.

2.2.4. Silicone Containing Crystal Violet and [$Au_{25}(Cys)_{18}$]: 224 mg of crystal violet was added into a mixture of [$Au_{25}(Cys)_{18}$] solution (28 mL), DI water (112 mL) and acetone (140 mL), and it was sonicated for 3 min. The silicone coupon was immersed in the mixture for 24 h and then it was washed by DI water twice. The washed silicone was stored in dark room for 24 h.

2.3. Bactericidal Test. The bactericidal activity of the silicone samples was tested against *Staphylococcus aureus* 8325-4 in the dark and in white light. One bacterial colony grown on mannitol salt agar (Oxoid) was inoculated into Brain Heart Infusion broth (BHI) and cultured in shaking incubator at 200 rpm at 37 ^{o}C. After 18 h culture, the bacteria were harvested using centrifugation. The centrifuge was operated with 2795×g at 20 ^{o}C for 5 min. The collected bacteria were washed with 10 mL of phosphate buffer saline (PBS). This process was performed twice to eliminate all traces of the broth. The bacteria suspension was diluted to get ~10^6 CFU/mL and 25 μL of each suspension was inoculated to the treated silicone, which was located in a colorless petri dish with water-saturated filter paper to maintain humidity. The silicone coupons were exposed to white light (Osram L58W/865 Lumilux) or maintained in the dark for the same time period before they were immersed in 450 μL of PBS and vortexed for 1 min to wash out bacteria from the silicone into the PBS. With ten-fold serial dilution, 100 μL of each dilution was plated onto mannitol salt agar and incubated at 37 ^{o}C for 24 h. The bacteria colonies that grew on the agar were counted.

2.4. UV-Vis Spectroscopy of Control and Treated Polymer. UV-Vis absorbance spectra of the treated silicones were obtained using a UV-Vis spectrometer (Lambda 25, PerkinElmer). The treated silicone coupons were placed onto the light wavelength detector and their absorbance spectra were determined in a range of 400 - 800 nm.

2.5. XPS and XRF Analysis. X-ray photoelectron spectroscopy (XPS) was used to investigate the $[Au_{25}(Cys)_{18}]$ within the treated silicone coupon or on its surface. The existence of gold was investigated after 0, 200 and 400 s of Ar ion sputtering. X-ray fluorescence spectroscopy (XRF, 15-watt Epsilon 4, Malvern Panalytical) was used to investigate the number of $[Au_{25}(Cys)_{18}]$ clusters inside the treated silicone. The polymer sample (Ø 7.0 cm × 0.04 cm) was placed into hollow of XRF and it was scanned for 15 min.

2.6. Leaching Test. The stability of silicone containing crystal violet and $[Au_{25}(Cys)_{18}]$ was investigated. The sample (1.5 cm × 1.5 cm × 0.04 cm) was placed in 5 mL of DI water for 20 days. To investigate leaching of crystal violet from the treated silicone, UV-Vis absorbance spectrum of the DI water was periodically obtained. Microwave plasma atomic emission spectroscopy (4210 MP-AES, Agilent Technologies) was employed to determine the concentration of Au in the DI water solution. After dipping the treated sample in 5 mL of DI water for 20 days, the solution was evaporated, and the solid obtained after evaporation was digested in 0.5 mL of *aqua regia* ($HCl:HNO_3$ 3:1 v:v). After digestion, the sample was diluted by DI water (final volume of 5 mL, water:*aqua regia* 9:1 v:v), and the gold content was determined via MP-AES.

2.7. Steady State Photoluminescence Spectroscopy. Photoluminescence (PL) spectra of control and treated polymers were measured using a photoluminescence spectrometer (FluoroMax, Horiba Scientific). A laser source with a wavelength of 574 nm was employed for

irradiation of the treated silicone and fluorescence was measured over a wavelength of 620-820 nm.

2.8. Time-Resolved Photoluminescence Spectroscopy. Time-resolved photoluminescence (PL) spectroscopy was operated using a time-correlated single photon counting (TCSPC) apparatus (DeltaFlex, Horiba Scientific). Pulsed 574 nm excitation by a laser diode (NanoLED-570) was used and fluorescence was measured at a wavelength of ~710 nm (Picosecond Photon Detection Module, PPD-900, Horiba Scientific) for 100 ns.

2.9. Statistical Analysis. Statistical T-test of experimental data was conducted by SPSS statistics (IBM Corporation).

3. RESULTS AND DISCUSSION

In $[Au_{25}(Cys)_{18}]$ synthesis, Au concentration in the precursor solution containing cysteine, chloroauric acid and NaOH was 10 mM, the molar ratio of Au-to-cysteine was 1:1.5 and the pH of the solution was maintained at 12. The color of the precursor changed from yellow to dark brown after passing through the reactor. The experiments were carried out at 60, 80 and 100 ℃ with different reaction (residence) times to determine an optimal condition of $[Au_{25}(Cys)_{18}]$ synthesis. As shown in Figure 2a), the UV-Vis absorbance features of $[Au_{25}(Cys)_{18}]$ gradually formed at 60 ℃ over 10 min of reaction time. The UV-Vis spectrum showed absorbance peaks at 450, 550, 670 and 770 nm, which agrees with the spectrum of $[Au_{25}(Cys)_{18}]$ from previous literature [26]. At 80 ℃, the absorption peaks of $[Au_{25}(Cys)_{18}]$ were clearly observed at 3 min. Subsequently, the absorbance at 670 nm stayed almost constant, but that at 610 nm gradually increased with reaction time, suggesting decomposition of $[Au_{25}(Cys)_{18}]$ (Figure 2b). At 100 ℃ the spectrum features of $[Au_{25}(Cys)_{18}]$ were observed after 1 min. However, the peaks gradually disappeared with increasing reaction time (Figure 2c). Since the absorbance peak at 670 nm is related to the amount of $[Au_{25}(Cys)_{18}]$ in the

solution [6, 26-27], the absorbance of each spectrum at 670 nm was plotted in terms of the reaction time. As shown in Figure 1d, the reaction at 80 ℃ produced higher concentration of $[Au_{25}(Cys)_{18}]$ than that at 60 and 100 ℃. Thus, it was concluded that $[Au_{25}(Cys)_{18}]$ clusters are most efficiently synthesized at 3 min reaction of the precursor in the reactor at 80 ℃, because the clusters could be rapidly synthesized while minimizing decomposition. To determine the robustness of the continuous system for $[Au_{25}(Cys)_{18}]$ synthesis, an 8 h continuous synthesis experiment was carried out at optimal conditions, i.e., 3 min reaction time at 80℃. The solution from the reactor outlet was collected at intervals of 2 h and its absorbance spectrum was measured using a UV-Vis spectrometer. UV-Vis spectra (Fig. 2e) show that the quality of $[Au_{25}(Cys)_{18}]$ synthesized during 8 h operation was constant. High-angle annular dark-field scanning transmission electron microscopy (HAADF-STEM) confirmed that $[Au_{25}(Cys)_{18}]$ clusters were <1 nm in diameter (Fig. 2f).

The molecular composition of $[Au_{25}(Cys)_{18}]$ was investigated by electrospray ionization mass spectrometry (ESI-MS). As shown in Figure 3a and 3b, one group of intense peaks at m/z ~2361.4 was observed and the peak at m/z 2361.4 (peak #1) was accompanied with a group of small peaks (#2-12). Analysis of isotope pattern at peak #1 confirmed that peak interval of ^{12}C and ^{13}C was 0.33 indicating $[Au_{25}(Cys)_{18}\text{-}3H]^{3-}$ generation (Figure 3c). The small peaks (#2-12) correspond to $[Au_{25}(Cys)_{18}]$ dissociated with H+ or coordinated with Na+, K+ or Cs+ which are common contaminant ions in ESI-MS [28-29]. Another group of $[Au_{25}(Cys)_{18}]$ peaks were observed at m/z ~ 1808.6 indicating 4- charged gas phase ions. Based on the optical density of the clusters at 670 nm and molar adsorption coefficient from literature [26-27] the yield of the $[Au_{25}(Cys)_{18}]$ was estimated to be ~95%.

In contrast with synthetic methods that use $NaBH_4$ as a reductant for Au nanoclusters synthesis, gaseous CO can be readily removed from the reaction solution through venting and it could

prevent potential boron contamination when using $NaBH_4$. In $[Au_{25}(Cys)_{18}]$ synthesis, cysteine reduces Au (III) ions to Cys-Au (I) complexes in solution at room temperature and increasing the pH of the solution with NaOH results in enhancement of the reduction ability of CO [26, 30]. $Au_{10\text{-}15}$ nanoclusters form from Cys-Au (I) through CO reduction and then Au_{25} nanoclusters develop through further growth *via* $Au_{16\text{-}25}$ nanoclusters [26]. In previous work, use of CO as reducing agent showed that high purity $[Au_{25}(Cys)_{18}]$ can be synthesized with high yield (~95%), but 24 h reaction time was employed to obtain the thiolated Au nanoclusters [26, 31]. Our continuous synthesis method showed that CO reduction of Cys-Au (I) within the reactor at elevated temperature significantly accelerated the production of $[Au_{25}(Cys)_{18}]$, and that 3 min residence time of the precursor at 80 ^{o}C was optimal, demonstrating that our experimental conditions produce high purity $[Au_{25}(Cys)_{18}]$ ~500 times faster than previous study [26]. The small diameter of the membrane reactor (~1 mm) allows for efficient temperature control and CO mass transfer, helping to intensify the $[Au_{25}(Cys)_{18}]$ synthesis.

To determine the photobactericidal enhancement by $[Au_{25}(Cys)_{18}]$, silicone containing $[Au_{25}(Cys)_{18}]$ and CV was produced through a swell-encapsulation-shrink process. When silicone is immersed in the swelling solution for 24 h, the polymer swells and crystal violet molecules and $[Au_{25}(Cys)_{18}]$ nanoclusters penetrate within the polymer matrix. After removal from the solution, the polymer shrinks resulting in CV and $[Au_{25}(Cys)_{18}]$ being encapsulated inside the silicone. To characterize the penetration process of CV into silicone, samples were prepared with various encapsulation times and then were thinly sliced. The side section of sliced samples was imaged and analyzed using ImageJ. Figure 4a shows CV profiles within the silicone with increasing encapsulation time. At the beginning, penetration of crystal violet was higher near the surface, while CV diffused throughout the polymer with increase of encapsulation time. CV diffusing through the polymer reached saturation by 24 h. Figure 4b shows XPS spectra of $[Au_{25}(Cys)_{18}]$ treated silicone after 0, 200 and 400 s of Ar ion sputtering.

A double peak at 87 and 83 eV, which corresponds to Au $4f_{5/2}$ and $4f_{7/2}$ was obtained at the surface and within the polymer bulk indicating successful encapsulation of $[Au_{25}(Cys)_{18}]$ into the silicone. XRF analysis indicated that ~6.49×10^{14} $[Au_{25}(Cys)_{18}]$ clusters/cm^3 were present within the silicone samples produced by 24 h encapsulation. Figure 4c exhibits UV-Vis absorption spectra of the silicone pieces over the wavelength of 400−800 nm. $[Au_{25}(Cys)_{18}]$ treated silicone did not show any change of the absorbance spectrum compared to the control. However, the CV treated silicone samples had a main absorption at 595 nm with shoulder peak at 540 nm. The main absorption of the polymer containing CV&$[Au_{25}(Cys)_{18}]$ was 1.7 times higher than the silicone with CV only.

The bactericidal activity of treated silicone was tested against *Staphylococcus aureus* 8325-4, a representative Gram-positive bacterium, in the dark and in white light. As shown in Figure S2, the intensity of the white light (Osram L58W/865 Lumilux) ranged from 200 to 429 lux (0.03 to 0.06 mW/cm^2) and the emission wavelength of the light source ranged from 400 to 800 nm. Figure 5 shows the bactericidal activity of the treated silicone in the dark and white light. In the dark, no reduction in viable bacteria number was apparent on any of the treated polymers compared to the control. After 6 h irradiation with white light, there was no reduction in the number of viable bacteria on the polymers containing either CV or $[Au_{25}(Cys)_{18}]$ alone. However, silicone containing CV and $[Au_{25}(Cys)_{18}]$ showed a significant reduction ($P<0.01$) in the number of bacteria to below the detection limit ($<10^2$ CFU/mL) after 6 h irradiation with white light, which equates to > 4.29 log reduction in viable bacterial numbers.

Previous study reported that negatively charged $[Au_{25}(Cys)_{18}]$ did not induce reactive oxygen species (ROS) but it showed an intrinsic bactericidal activity[32]. This might be because the negatively charged nanocluster acts as a radical. However, the negative charged nanocluster can be neutralized through air oxidation[33]. In this study, negatively charged $[Au_{25}(Cys)_{18}]$

which was incorporated into silicone did not show bactericidal activity in dark. This can be explained by the fact that as negative charged $[Au_{25}(Cys)_{18}]$ nanoclusters encapsulated into silicone are exposed to air, the nanoclusters are neutralized resulting in a loss of their disinfection feature.

With respect to photobactericidal activity, crystal violet has been known for inducing visible light active photocatalysis[13]. When crystal violet molecules are exposed to visible light, the molecules transform to a triplet state from a ground state *via* an excited singlet state[19, 34-35]. Through photochemical reaction type-I or/and type-II, CV molecules in a triplet state induce ROS generation leading to bacteria death[13, 19, 34-36]. In this study, crystal violet treated polymer did not show any bactericidal activity in white light. However, addition of $[Au_{25}(Cys)_{18}]$ into the treated polymer activated potent bactericidal activity in identical conditions. To determine the interaction between CV and $[Au_{25}(Cys)_{18}]$ in white light, steady state photoluminescence (PL) spectroscopy and time-resolved PL spectroscopy were used. Figure 6a shows the PL spectra of control, polymers with CV only and $[Au_{25}(Cys)_{18}]$ only. Upon illumination at ~574 nm, silicone containing CV only exhibited a PL spectrum with a peak at ~688 nm, while compared to control, silicone with $[Au_{25}(Cys)_{18}]$ only did not show a distinctive spectrum, indicating that $[Au_{25}(Cys)_{18}]$ within the silicone might not be photoexcited, as further supported by a phosphorescence study of silicone with $[Au_{25}(Cys)_{18}]$ only (Figure S3). Figure 6b shows time-resolved PL decay of control and treated silicone samples. Upon 574 nm laser excitation, the PL decay was measured at a wavelength of 710 nm. The curve of silicone containing $[Au_{25}(Cys)_{18}]$ only was similar to that of control. The polymer with CV only showed a longer PL lifetime than that of control and silicone with $[Au_{25}(Cys)_{18}]$ only after the laser excitation. After $[Au_{25}(Cys)_{18}]$ addition into CV treated silicone, the PL lifetime of the silicone became shorter, indicating that some excited electrons in CV flow to $[Au_{25}(Cys)_{18}]$. It is suggested that after light illumination, photoexcited electrons within CV transfer to $[Au_{25}(Cys)_{18}]$, which acts

as electron receptor, and as electrons accumulate on [$Au_{25}(Cys)_{18}$] they interact with molecular oxygen, resulting in redox reaction enhancement [37-38].

To investigate the stability of the treated silicone, CV and [$Au_{25}(Cys)_{18}$] leaching from the polymer was evaluated and cyclic testing of photobactericidal activity was performed. A silicone sample containing CV&[$Au_{25}(Cys)_{18}$] was immersed in DI water and CV leaching was regularly measured using a UV-Vis spectrometer (Figure S4a). The release of [$Au_{25}(Cys)_{18}$] from the polymer was measured after 20 days immersion. The concentrations of gold and CV in the DI water that leached from the polymer was ~0.24 and ~0.06 ppm respectively, indicating that the leaching was minor. In the cyclic photobactericidal test, three samples were tested with a *S. aureus* 8325-4 suspension containing ~10^5 CFU/mL. Photobactericidal test on each sample was performed five times and at each time, any changes in photobactericidal activity of silicone with CV&[$Au_{25}(Cys)_{18}$] was determined. As shown in Figure S4b, at the beginning, the silicone sample showed potent photobactericidal activity with 99.9 % reduction of viable bacteria. After two cycles, the bactericidal activity was slightly reduced but the sample still showed a photobactericidal effectiveness of between 82 to 91%.

In our previous studies, continuous two-phase synthesis for [$Au_{25}(Cys)_{18}$] (where CO first saturated an organic segmenting fluid, and then transferred to the aqueous precursor solution) and its photobactericidal enhancement was reported [29, 39]. As shown in Figure S5, [$Au_{25}(Cys)_{18}$] nanoclusters synthesized in the present study by the single-phase method showed higher photobactericidal activity than those synthesized by the two-phase method in identical conditions. This indicates that the single-phase synthetic method may produce higher purity [$Au_{25}(Cys)_{18}$] than the two-phase synthetic method. Contrary to the single-phase method, heptane was used as CO reservoir in the two-phase method because heptane has higher CO

solubility than water[29]. Although heptane was removed after [$Au_{25}(Cys)_{18}$] synthesis, very small quantity might have remained and affected the [$Au_{25}(Cys)_{18}$] purity in the solution.

Previous studies showed that addition of nanoparticles rendered UV-active photocatalysts active under a longer wavelength of light and enhanced the photobactericidal activity of polymers containing photosensitizers under white light [20-25, 40]. However, use of an intense white light or laser source was required to achieve potent bactericidal activity [20-25, 40]. Au nanoclusters do not have plasmonic behavior, and they have a discontinuous band structure indicating a discrete energy level compared to Au nanoparticles [1-2]. In this study, it was observed that [$Au_{25}(Cys)_{18}$] addition into CV treated silicone led to a potent bactericidal activity (> 4.29 log reduction in viable bacteria) against *S. aureus* after 6 h exposure at low white light flux. This indicates that the nanoclusters are a more efficient photocatalytic enhancer than metal nanoparticles and it is expected that this combination can be applied for indoor facilities because the intensity of white light in most indoor locations ranges from 200 to 1000 lux (0.03 to 0.15 mW/cm^2) [41-42].

4. CONCLUSION

A continuous single-phase synthetic method for [$Au_{25}(Cys)_{18}$] was developed in this study using carbon monoxide as a reductant. Our method enables the robust production of high quality [$Au_{25}(Cys)_{18}$] nanoclusters within 3 min. This is achieved by operating at elevated temperature with a small channel membrane reactor. [$Au_{25}(Cys)_{18}$] addition into crystal violet treated polymer successfully activated a potent photobactericidal activity at a low flux levels of white light. Steady state and time-resolved photoluminescence spectroscopy showed that after light irradiation, photoexcited electrons within crystal violet flowed to [$Au_{25}(Cys)_{18}$] in the silicone. It is suggested that redox reaction from [$Au_{25}(Cys)_{18}$] enhanced the photobactericidal activity. This study demonstrates not only an efficient method for

$[Au_{25}(Cys)_{18}]$ synthesis which is fast, simple and scalable, but also the application of $[Au_{25}(Cys)_{18}]$ in photocatalysis research.

■ ASSOCIATED CONTENT

Supporting Information

The Supporting Information is available free of charge

Crystallographic structure of $[Au_{25}(Cys)_{18}]$, Intensity distribution and emission wavelength of white light, Time-resolved $^1O_2$ phosphorescence decay of treated silicones, Stability test of treated silicones, and Comparison of photobactericidal enhancement by $[Au_{25}(Cys)_{18}]$ nanoclusters synthesized through two different synthetic methods

■ AUTHOR INFORMATION

Corresponding Authors

Asterios Gavriilidis - *Department of Chemical Engineering, University College London, London, Torrington Place, London, WC1E 7JE, United Kingdom;* E-mail: a.gavriilidis@ucl.ac.uk

Ivan P. Parkin - *Materials Chemistry Research Centre, Department of Chemistry, University College London, 20 Gordon Street, London, WC1H 0AJ*, *United Kingdom*; E-mail: i.p.parkin@ucl.ac.uk

Other Authors

[t]Gi Byoung Hwang - *Materials Chemistry Research Centre, Department of Chemistry, University College London, 20 Gordon Street, London, WC1H 0AJ, United Kingdom.*

[t] Gaowei Wu - *Department of Chemical Engineering, University College London, Torrington Place, London, WC1E 7JE, United Kingdom*

Juhun Shin - *Materials Chemistry Research Centre, Department of Chemistry, , University College London, 20 Gordon Street, London, WC1H 0AJ, United Kingdom.*

Luca Panariello - *Department of Chemical Engineering, University College London, Torrington Place, London, WC1E 7JE, United Kingdom*

Victor Sebastian - *Nanoscience Institute of Aragon, Aragón Materials Science Institute, ICMA, CSIC and Chemical and Environmental Engineering Department, University of Zaragoza, 50018 Zaragoza, Spain*

Kersti Karu- *Materials Chemistry Research Centre, Department of Chemistry, University College London, 20 Gordon Street, London, WC1H 0AJ, United Kingdom.*

Elaine Allan - *Department of Microbial Diseases, UCL Eastman Dental Institute, University College London, 256 Grays Inn Road, London, WC1X 8LD, United Kingdom*

Author Contributions

The manuscript was written through contributions of all authors. All authors have given approval to the final version of the manuscript.

[t] These authors contributed equally. (match statement to author names with a symbol)

Conflict of interest

The authors declare no competing financial interest.

■ACKNOWLEDGEMENTS

The authors thank the EPSRC for financial support (EP/M015157/1) through the Manufacturing Advanced Functional Materials (MAFuMa) scheme. LP received funding from the European Union's Horizon 2020 research and innovation programme under the Marie Skłodowska-Curie grant agreement No 721290. This publication reflects only the authors' view, exempting the Community from any liability. Project website: http://cosmic-etn.eu/. VS acknowledges the LMA-INA for offering access to their instruments and the financial support of Ministerio de Ciencia, Innovación y Universidades, Programa Retos Investigación, Proyecto REF: RTI2018-099019-A-I00

■ABBREVIATIONS

TBO, toluidine blue O
MB, methylene blue
CV, crystal violet
NP, nanoparticles
ESI-MS, electrospray ionization mass spectrometry
PL, photoluminescence

■ REFERENCES

(1) Kang, X.; Chong, H.; Zhu, M. $Au_{25}(SR)_{18}$: The Captain of the Great Nanocluster Ship. *Nanoscale* **2018,** *10*, 10758-10834.
(2) Jin, R. Atomically Precise Metal Nanoclusters: Stable Sizes and Optical Properties. *Nanoscale* **2015,** *7*, 1549-1565.
(3) Yuan, X.; Zhang, B.; Luo, Z.; Yao, Q.; Leong, D. T.; Yan, N.; Xie, J. Balancing the Rate of Cluster Growth and Etching for Gram-Scale Synthesis of Thiolate-Protected Au_{25} Nanoclusters with Atomic Precision. *Angew. Chem. Int. Ed. Engl.* **2014,** *53*, 4623-4627.
(4) Jin, R.; Zeng, C.; Zhou, M.; Chen, Y. Atomically Precise Colloidal Metal Nanoclusters and Nanoparticles: Fundamentals and Opportunities. *Chem. Rev.* **2016,** *116*, 10346-10413.
(5) Zhu, M.; Lanni, E.; Garg, N.; Bier, M. E.; Jin, R. Kinetically Controlled, High-Yield Synthesis of Au_{25} Clusters. *J. Am. Chem. Soc.* **2008,** *130*, 1138-1139.
(6) Chen, T.; Yao, Q.; Yuan, X.; Nasaruddin, R. R.; Xie, J. Heating or Cooling: Temperature Effects on the Synthesis of Atomically Precise Gold Nanoclusters. *J. Phys. Chem. C* **2016,** *121*, 10743-10751.
(7) Katla, S. K.; Zhang, J.; Castro, E.; Bernal, R. A.; Li, X. Atomically Precise $Au_{25}(SG)_{18}$ Nanoclusters: Rapid Single-Step Synthesis and Application in Photothermal Therapy. *ACS Appl. Mater. Interfaces* **2018,** *10*, 75-82.
(8) Yuan, X.; Yu, Y.; Yao, Q.; Zhang, Q.; Xie, J. Fast Synthesis of Thiolated Au_{25} Nanoclusters via Protection-Deprotection Method. *J. Phys. Chem. Lett.* **2012,** *3*, 2310-2314.
(9) Negishi, Y.; Sakamoto, C.; Ohyama, T.; Tsukuda, T. Synthesis and the Origin of the Stability of Thiolate-Protected Au_{130} and Au_{187} Clusters. *J. Phys. Chem. Lett.* **2012,** *3*, 1624-1628.
(10) Goswami, N.; Yao, Q.; Chen, T.; Xie, J. Mechanistic Exploration and Controlled Synthesis of Precise Thiolate-Gold Nanoclusters. *Coord. Chem. Rev.* **2016,** *329*, 1-15.
(11) Jin, R.; Qian, H.; Wu, Z.; Zhu, Y.; Zhu, M.; Mohanty, A.; Garg, N. Size Focusing: A Methodology for Synthesizing Atomically Precise Gold Nanoclusters. *J. Phys. Chem. Lett.* **2010,** *1*, 2903-2910.
(12) Wu, Z.; Suhan, J.; Jin, R. One-Pot Synthesis of Atomically Monodisperse, Thiol-Functionalized Au_{25} Nanoclusters. *J. Mater. Chem.* **2009,** *19*, 622-626.
(13) Docampo, R.; Moreno, S. N.; Muniz, R. P.; Cruz, F. S.; Mason, R. P. Light-Enhanced Free Radical Formation and Trypanocidal Action of Gentian Violet (crystal violet). *Science* **1983,** *220*, 1292-1295.
(14) Matsunaga, T.; Tomoda, R.; Nakajima, T.; Wake, H. Photoelectrochemical Sterilization of Microbial Cells by Semiconductor Powders. *FEMS Microbiol. Lett.* **1985,** *29*, 211-214.
(15) Gupta, S. M.; Tripathi, M. A Review of TiO_2 Nanoparticles. *Chinese Sci. Bull.* **2011,** *56*, 1639-1657.
(16) Wang, Z. L. Zinc Oxide Nanostructures: Growth, Properties and Applications. *J. Phys. Condens. Matter* **2004,** *16*, R829-R858.
(17) Sirelkhatim, A.; Mahmud, S.; Seeni, A.; Kaus, N. H. M.; Ann, L. C.; Bakhori, S. K. M.; Hasan, H.; Mohamad, D. Review on Zinc Oxide Nanoparticles: Antibacterial Activity and Toxicity Mechanism. *Nano-Micro Lett.* **2015,** *7*, 219-242.
(18) Ozkan, E.; Allan, E.; Parkin, I. P. The antibacterial properties of light-ctivated polydimethylsiloxane containing crystal violet. *RSC Adv.* **2014,** *4*, 51711-51715.
(19) Wainwright, M. Photodynamic Antimicrobial Chemotherapy (PACT). *J. Antimicrob. Chemother.* **1998,** *42*, 13-28.

(20) Akhavan, O.; Abdolahad, M.; Abdi, Y.; Mohajerzadeh, S. Synthesis of Titania/Carbon Nanotube Heterojunction Arrays for Photoinactivation of *E. coli* in Visible Light Irradiation. *Carbon* **2009,** *47*, 3280-3287.
(21) Dalrymple, O. K.; Stefanakos, E.; Trotz, M. A.; Goswami, D. Y. A Review of the Mechanisms and Modeling of Photocatalytic Disinfection. *Appl. Catal. B* **2010,** *98*, 27-38.
(22) Hwang, G. B.; Noimark, S.; Page, K.; Sehmi, S.; Macrobert, A. J.; Allan, E.; Parkin, I. P. White Light-Activated Antimicrobial Surfaces: Effect of Nanoparticles Type on Activity. *J. Mater. Chem. B* **2016,** *4*, 2199-2207.
(23) Dunnill, C. W.; Aiken, Z. A.; Kafizas, A.; Pratten, J.; Wilson, M.; Morgan, D. J.; Parkin, I. P. White Light Induced Photocatalytic Activity of Sulfur-Doped TiO_2 Thin Films and their Potential for Antibacterial Application. *J. Mater. Chem.* **2009,** *19*, 8747-8754.
(24) Ganguly, P.; Byrne, C.; Breen, A.; Pillai, S. C. Antimicrobial Activity of Photocatalysts: Fundamentals, Mechanisms, Kinetics and Recent Advances. *Appl. Catal. B* **2018,** *225*, 51-75.
(25) Perni, S.; Prokopovich, P.; Piccirillo, C.; Pratten, J.; Parkin, I. P.; Wilson, M. Toluidine Blue-Containing Polymers Exhibit Potent Bactericidal Activity when Lrradiated with Red Laser Light. *J. Mater.Chem.* **2009,** *19*, 2715-2723.
(26) Yu, Y.; Luo, Z.; Yu, Y.; Lee, J. Y.; Xie, J. Observation of Cluster Size Growth in CO-Directed Synthesis of $Au_{25}(SR)_{18}$ Nanoclusters. *ACS Nano* **2012,** *6*, 7920-7927.
(27) Negishi, Y.; Nobusada, K.; Tsukuda, T. Glutathione-Protected Gold Clusters Revisited: Bridging the Gap Between Gold(I)-Thiolate Complexes and Thiolate-Protected Gold Nanocrystals. *J. Am. Chem. Soc.* **2005,** *127*, 5261-5270.
(28) Keller, B. O.; Sui, J.; Young, A. B.; Whittal, R. M. Interferences and Contaminants Encountered in Modern Mass Spectrometry. *Anal. Chim. Acta* **2008,** *627*, 71-81.
(29) Huang, H.; Hwang, G. B.; Wu, G.; Karu, K.; Du Toit, H.; Wu, H.; Callison, J.; Parkin, I. P.; Gavriilidis, A. Rapid Synthesis of $[Au_{25}(Cys)_{18}]$ Nanoclusters *via* Carbon Monoxide in Microfluidic Liquid-Liquid Segmented Flow System and their Antimicrobial Performance. *J. Chem. Eng.* **2020,** *383*, 123176.
(30) Yu, Y.; Chen, X.; Yao, Q.; Yu, Y.; Yan, N.; Xie, J. Scalable and Precise Synthesis of Thiolated $Au1_{0–12}$, Au_{15}, Au_{18}, and Au_{25} Nanoclusters via pH Controlled CO Reduction. *Chem. Mater.* **2013,** *25*, 946-952.
(31) Luo, Z.; Nachammai, V.; Zhang, B.; Yan, N.; Leong, D. T.; Jiang, D. E.; Xie, J. Toward Understanding the Growth Mechanism: Tracing All Stable Intermediate Species from Reduction of Au(I)-Thiolate Complexes to Evolution of Au_{25} nanoclusters. *J. Am. Chem. Soc.* **2014,** *136*, 10577-10580.
(32) Zheng, K.; Setyawati, M. I.; Leong, D. T.; Xie, J. Surface Ligand Chemistry of Gold Nanoclusters Determines their Antimicrobial Aility. *Chem. Mater.* **2018,** *30*, 2800-2808.
(33) Zhu, M.; Eckenhoff, W. T.; Pintauer, T.; Jin, R. Conversion of Anionic $[Au_{25}(SCH_2CH_2Ph)_{18}]^-$ Cluster to Charge Neutral Cluster via Air Oxidation. *J. Phys. Chem. C* **2008,** *112* (37), 14221-14224.
(34) Henderson, B. W.; Dougherty, T. J. How Does Photodynamic Therapy Work? *Photochem. Photobiol.* **1992,** *55*, 145-157.
(35) Vatansever, F.; de Melo, W. C.; Avci, P.; Vecchio, D.; Sadasivam, M.; Gupta, A.; Chandran, R.; Karimi, M.; Parizotto, N. A.; Yin, R.; Tegos, G. P.; Hamblin, M. R. Antimicrobial Strategies Centered Around Reactive Oxygen Species-Bactericidal Antibiotics, Photodynamic Therapy, and Beyond. *FEMS Microbiol. Rev.* **2013,** *37*, 955-989.
(36) Noimark, S.; Salvadori, E.; Gomez-Bombarelli, R.; MacRobert, A. J.; Parkin, I. P.; Kay, C. W. Comparative Study of Singlet Oxygen Production by Photosensitiser Dyes Encapsulated in Silicone: Towards Rational Design of Anti-Microbial Surfaces. *Phys. Chem. Chem. Phys.* **2016,** *18*, 28101-28109.

(37) Yang, Z.; Chen, L.; Yang, Y.; Wang, J.; Huang, Y.; Liu, X.; Yang, S. Constructing TiO_2 Decorated Bi_2WO_6 Architectures with Enhanced Visible-Light-Driven Photocatalytic Activity. *Semicond. Sci. Technol.* **2017,** *32*, 065008.
(38) Xu, J.; Feng, B.; Wang, Y.; Qi, Y.; Niu, J.; Chen, M. BiOCl Decorated $NaNbO_3$ Nanocubes: A Novel p-n Heterojunction Photocatalyst with Improved Activity for Ofloxacin Degradation. *Front. Chem.* **2018,** *6*, 393.
(39) Hwang, G. B.; Huang, H.; Wu, G.; Shin, J.; Kafizas, A.; Karu, K.; Toit, H. D.; Alotaibi, A. M.; Mohammad-Hadi, L.; Allan, E.; MacRobert, A. J.; Gavriilidis, A.; Parkin, I. P. Photobactericidal Activity Activated by Thiolated Gold Nanoclusters at Low Flux Levels of White Light. *Nat. Comm.* **2020,** *11*, 1207.
(40) Lan, Y.; Hu, C.; Hu, X.; Qu, J. Efficient Destruction of Pathogenic Bacteria with $AgBr/TiO_2$ under Visible Light Irradiation. *Appl. Catal.* **2007,** *73*, 354-360.
(41) Piano, E. Guidelines for Indoor Lighting in The Public and Private Service Sector. http://www.premiumlightpro.org.uk/fileadmin/uk/Premium_Light_Pro_Indoor_LED_Guidelines.pdf.
(42) Bukorović, N., Lighting Guide 2 - Hospitals and Health Care Buildings 2008. Chartered Institution of Building Services Engineers

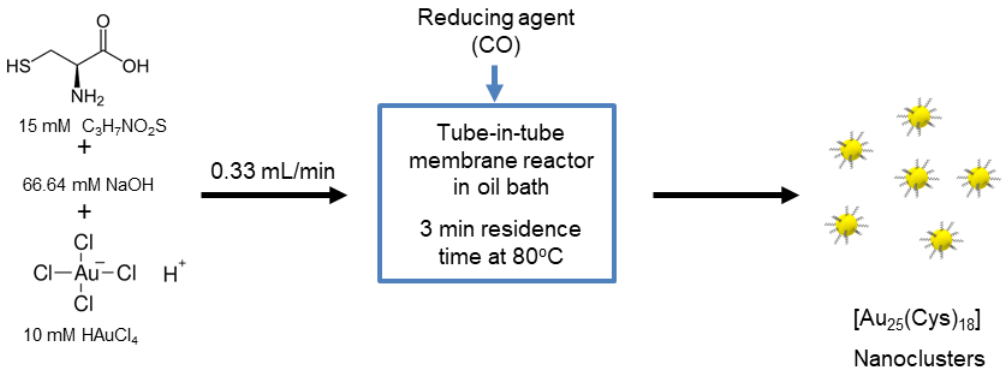

Scheme 1. [$Au_{25}(Cys)_{18}$] synthesis with a tube-in-tube membrane reactor.

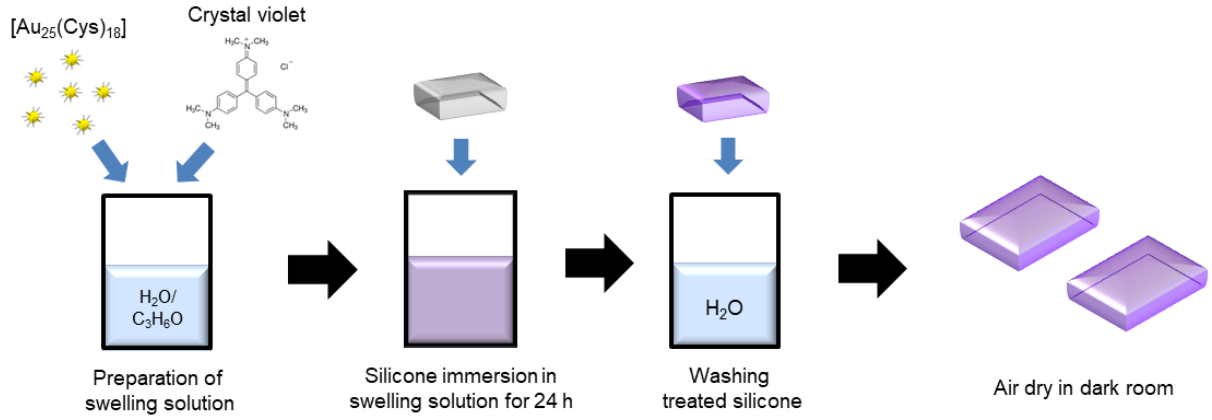

Scheme 2. Production of silicone coupons containing crystal violet and [$Au_{25}(Cys)_{18}$] through a swell-encapsulation-shrink process.

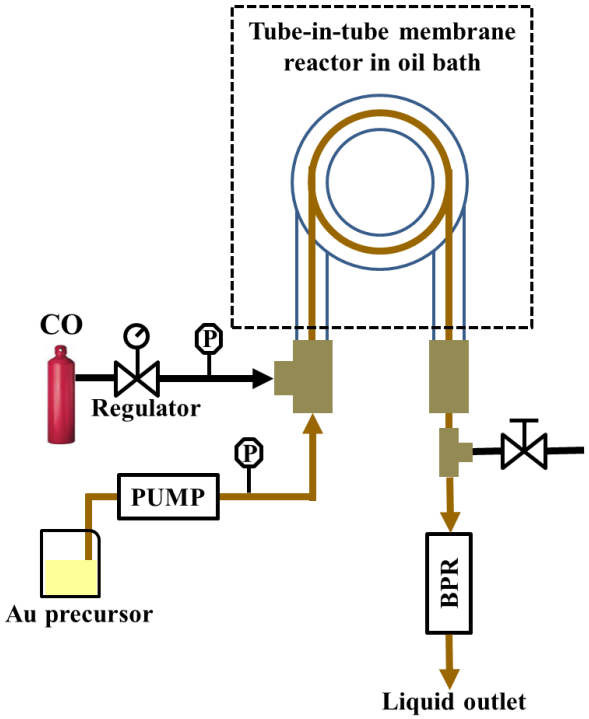

Figure 1. Schematic diagram of the Teflon AF-2400 tube-in-tube membrane reactor set-up (P: pressure sensor; BPR: back pressure regulator).

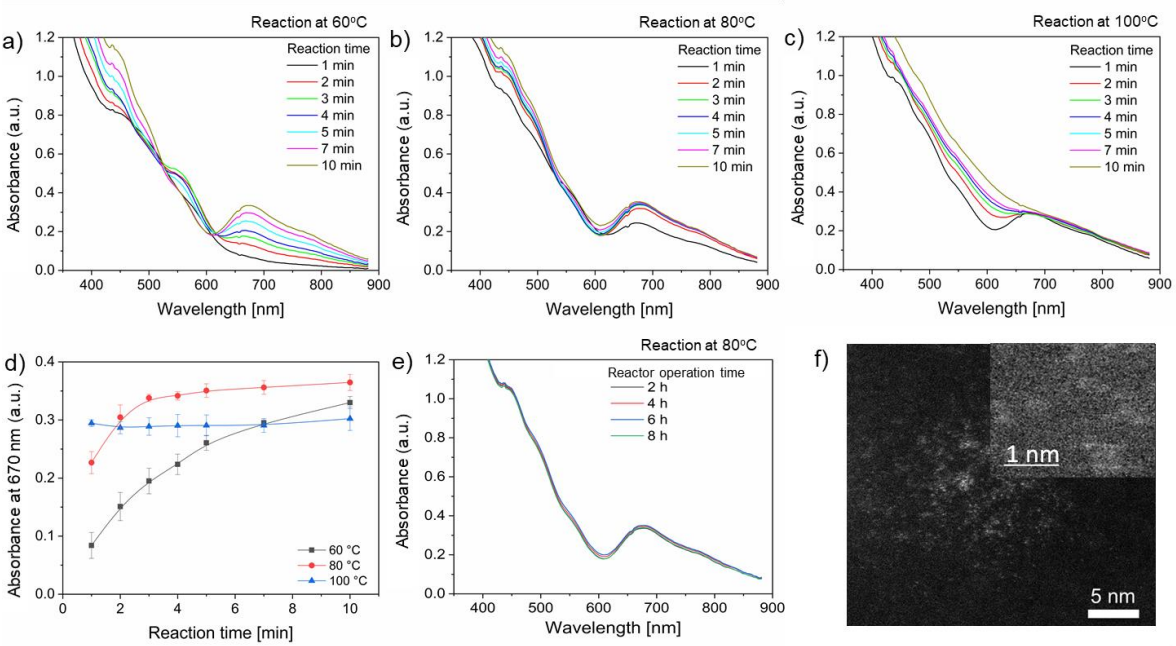

Figure 2. UV-Vis absorbance spectra of $[Au_{25}(Cys)_{18}]$ synthesized at a) 60 , b) 80 and c) 100 °C with increasing reaction time, d) changes of absorbance of $[Au_{25}(Cys)_{18}]$ clusters at 670 nm at 60 °C, 80 °C and 100 °C with increasing reaction time, e) UV-Vis absorbance spectra of $[Au_{25}(Cys)_{18}]$ synthesized during an 8 h long experiment (reaction time: 3 min, reaction temperature: 80 °C) and f) image of $[Au_{25}(Cys)_{18}]$ taken by HAADF-STEM. White dots indicate $[Au_{25}(Cys)_{18}]$ nanoclusters.

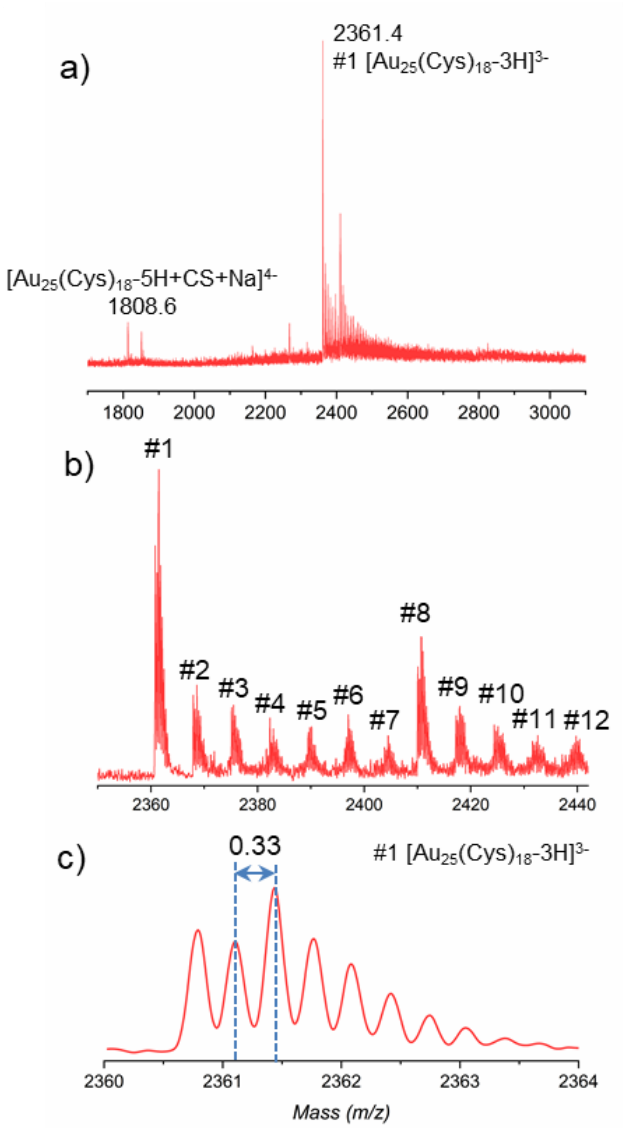

Figure 3. ESI mass spectra of synthesized [$Au_{25}(Cys)_{18}$]: a) full-range spectra, b) zoomed-in spectra in the m/z range of 2360-2440 and c) isotope pattern of #1 peak

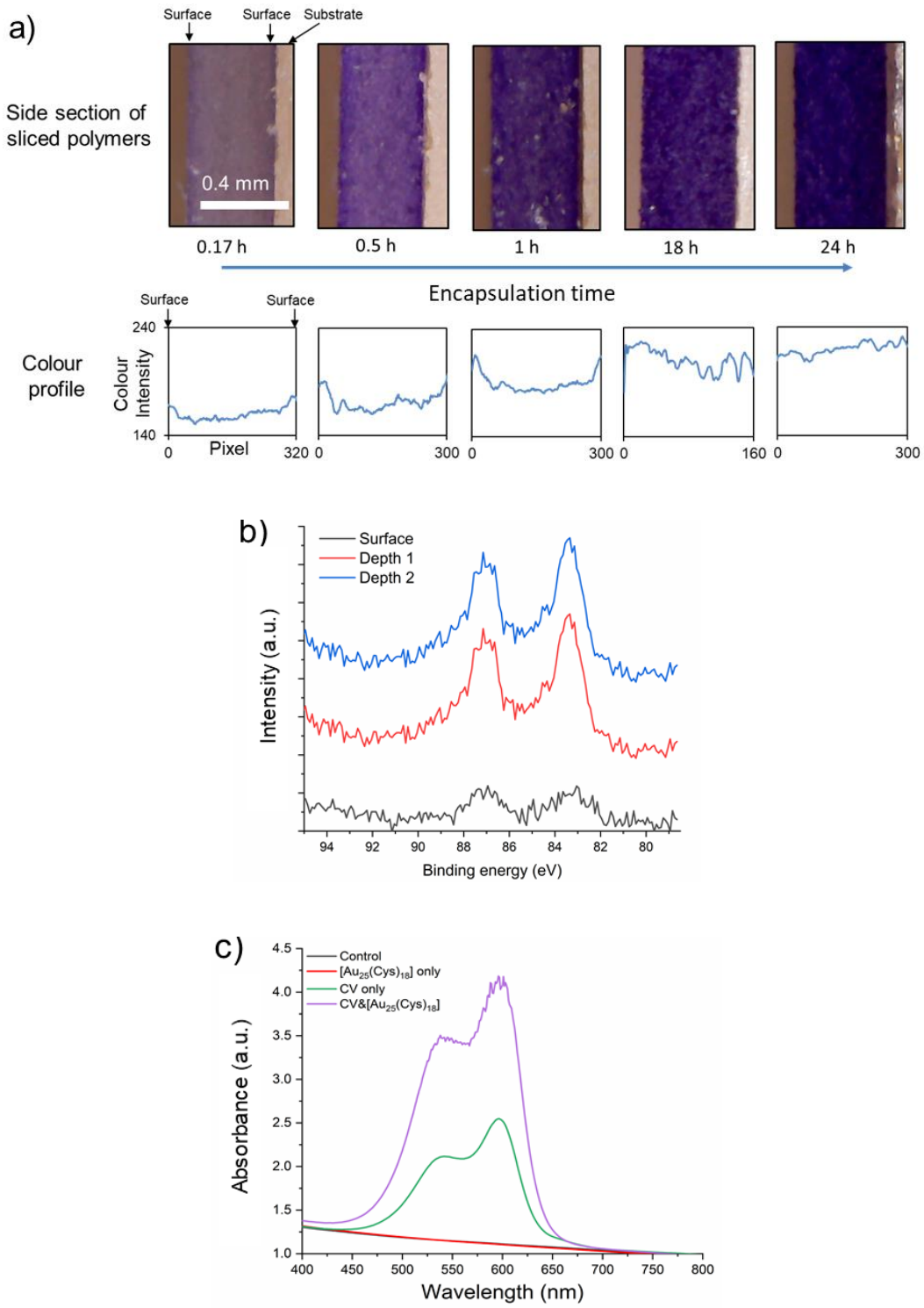

Figure 4. a) Crystal violet (CV) distribution in thinly sliced silicone after 0.17, 0.5, 1, 18, and 24 h encapsulation time, b) XPS depth profile for analysis of gold inside a silicone sample with CV&[$Au_{25}(Cys)_{18}$)]; Surface, Depth 1 and Depth 2 indicate measurements after 0, 200 and 400 s of Ar ion sputtering respectively, c) UV-Vis absorbance spectra of untreated silicone (Control), silicone with [$Au_{25}(Cys)_{18}$] only, silicone with CV only and silicone with CV&[$Au_{25}(Cys)_{18}$] at a wavelength of 400−800 nm.

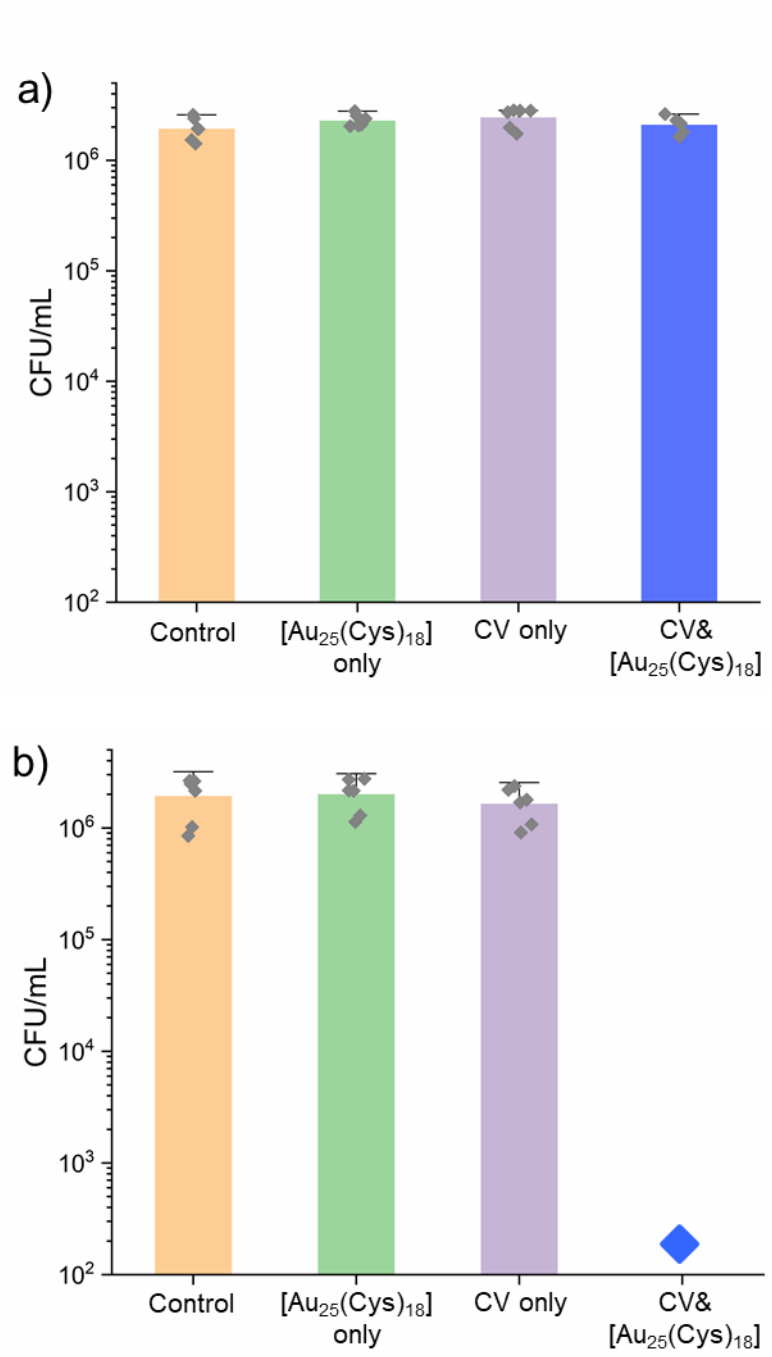

Figure 5. Bactericidal activity of untreated silicone (Control), silicone with $[Au_{25}(Cys)_{18}]$ only, silicone with CV only and silicone with CV&$[Au_{25}(Cys)_{18}$ against *S. aureus* 8325-4 after 6 h irradiation time in a) dark and b) white light (n = 6 samples) at 20 °C.

◆ Below detection limit: $<10^2$ CFU/mL

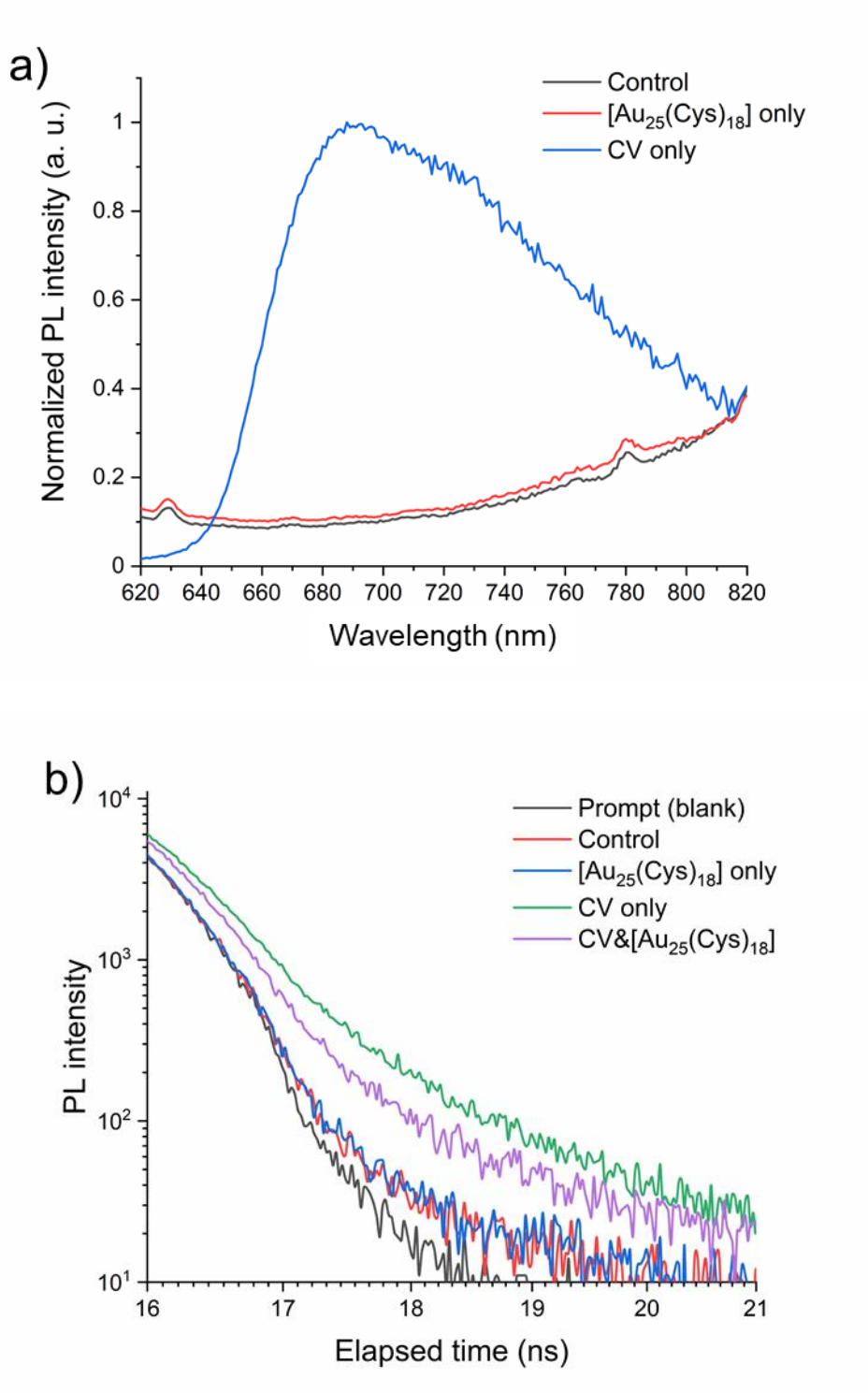

Figure 6. a) Steady state photoluminescence (PL) spectra of untreated silicone (Control), silicone with $[Au_{25}(Cys)_{18}]$ only and silicone with CV only (λ_{Ex} = 574 nm). b) Time-resolved photoluminescence (PL) decay of untreated silicone (Control), silicone with $[Au_{25}(Cys)_{18}]$ only, silicone with CV only and silicone with CV&$[Au_{25}(Cys)_{18}]$ (λ_{Ex} = 574 nm, λ_{Em} = 710 nm).

TOC/Abstract Graphics